Hindawi Publishing Corporation
Mathematical Problems in Engineering
Volume 2015, Article ID 586913, 17 pages
http://dx.doi.org/10.1155/2015/586913

Research Article

Comparative Study of Radiative Effects on Double Diffusive Convection in Nongray Air-CO_2 Mixtures in Cooperating and Opposing Flow

Siham Laouar-Meftah,[1] Denis Lemonnier,[2] Didier Saury,[2] Abderrahmane Benbrik,[1] and Mohamed Cherifi[1]

[1] *Faculty of Hydrocarbon and Chemistry, M'Hamed Bougara University, 35000 Boumerdes, Algeria*
[2] *Institut Pprime, CNRS, ENSMA, University of Poitiers, Futuroscope, 86961 Chasseneuil, France*

Correspondence should be addressed to Siham Laouar-Meftah; laouarmeftah@gmail.com

Received 10 September 2014; Revised 27 January 2015; Accepted 28 January 2015

Academic Editor: Pedro Jorge Martins Coelho

This study analyses the effects of nongray gas radiation on double diffusive convection, in a square differentially heated cavity filled with air-CO_2 mixtures, when the buoyancy forces (thermal and mass) are cooperating or opposing. The radiative source term in the energy equation is evaluated by the discrete ordinate method (solving the radiative transfer equation) and the SLW spectral model (accounting for real radiative properties of absorbing species). Here, gas absorption varies with the local temperature and concentration of pollutant, which induces a strong direct coupling between the concentration and thermal fields that would not exist with gray gas. Simulations are performed at different concentrations of CO_2 corresponding to different flow regimes (thermal, transitional, and mass). Results show the following: (i) in cooperating flow, radiation modifies essentially the heat transfer and the characteristics of temperature and concentration fields; (ii) in opposing flow, radiation effects are more important and depend on the nature of the flow regime.

1. Introduction

Radiation heat transfer occurs in many engineering applications (cooling electronic components, nuclear reactors, industrial furnaces, combustion chambers, and so on) where it is coupled to other modes of heat transfer, like conduction and natural or forced convection. It can be substantial even at temperatures as low as 273 K [1, 2] and its influence on natural convection is more important than on forced convection [3] (because of direct coupling between thermal and dynamic fields in natural convection). Many investigations dealing with coupling natural convection and radiation in cavities [4–7] have been conducted with a transparent medium (only surface-to-surface radiation interaction, acting indirectly through heat flux boundary conditions at passive walls). However, many real engineering problems involve truly absorbing-emitting gases. In this case, volumetric radiation can significantly affect the temperature field which, in turn, induces changes in the fluid dynamic. Among works discussing the natural convection-radiation interaction in a confined semitransparent space, many use the simple assumption of a gray fictitious gas [8–11]. This approach is very unlikely to depict real situations, because the radiative transfer in a semitransparent medium (particularly in gases) depends on radiative properties of fluid that vary with the wavelength, the temperature, and the concentration (or partial pressure) of radiating species. It is noted that the absorption spectra of gases have very strong dynamics, consisting of hundreds of thousands of lines, with variables intensity and multiple quasitransparent bands between them. For these reasons, no (real) gas can be properly represented by a gray model, wherein an average value of the absorption coefficient of the spectrum is considered.

Among the first works taking into account nongray radiative properties of the fluid, we cite the analytical and

experimental study of Bratis and Novotny [12] in a differentially heated rectangular enclosure filled with a NH_3-N_2 gas mixture. The same problem was treated by Fusegi and Farouk [13] in 2D and Fusegi et al. [14] in a 3D thermal driven cavity filled with CO_2. The authors used the simplest nongray model, named weighted sum of gray gas model (WSGG), to account for the spectral aspect of the radiative transfer. Colomer et al. [15] also studied this coupled transfer phenomenon (in CO_2, H_2O, and CO_2-H_2O mixtures) using the SLW spectral model (spectral line weighted sum of gray gases), which is considered as a refinement to the WSGG model. They concluded that the use of any of the nongray models is justified since neither the gray gas nor the transparent model captures well the real gas behavior. Recently, Soucasse et al. [16] and Ibrahim et al. [17] considered the same coupled phenomena in laminar regime for a 3D cavity filled with an air/CO_2/H_2O mixture [16] and in turbulent regime for a 2D cavity filled with an air-H_2O mixture [17]. The spectral dependency of gas radiative properties is handled by the global ADF model [16] and the SLW model [17] (the two models are similar in their principle). Regarding the coupling of radiation with the double diffusive natural convection, most of the available investigations use the simple assumption of fictitious gray medium (uniform absorption over space and wavelengths) [18–21]. In these works, the fluid was generally regarded as optically thick and the radiative fluxes were calculated by using the Rosseland approximation. Rafieivand [22], Mezrhab et al. [23], and Moufekkir et al. [24] have investigated the same coupling phenomena in a gas mixture. They considered a more realistic situation of an absorption coefficient of fluid proportional to the local concentration of the absorbing species. These studies are still limited to the gray gas assumption.

Recently, some attempts have been made to study double diffusive convection coupled to radiation in participating gases, accounting for the real (nongray) radiative properties of the mixture (absorption varies with temperature, concentration, and wavelength). In this context, we can mention the numerical studies performed by Meftah et al. [25] and Laouar-Meftah et al. [26] in a stationary laminar flow of air-CO_2 (or air-H_2O) gas mixtures and Ibrahim and Lemonnier [27] in transient laminar flow of N_2-CO_2 mixture. The authors used the SLW spectral model of Denison and Webb [28] along with the discrete ordinate method to account for the real radiative participation of the medium. Here, as gas absorption varies with the local temperature and concentration of pollutant, a strong direct coupling between the concentration and thermal fields occurs, which does not exist with gray gas. There is a direct influence on the thermal field (through a volumetric heat source in energy equation) and an indirect influence on the dynamic field (by modifying buoyancy forces) and the field of concentration (through the dynamic field). In turn, these fields (T and C) influence the radiative transfer through absorbing properties of radiating species, characterized by the absorption coefficient κ which depends, in particular, on the local concentration of pollutant. Therefore, the objective of our investigation is to highlight the effect of nongray gas radiation on natural double diffusive convection (flow structures, heat and mass transfer, and so on) in the three convective flow regimes: thermal, intermediate, and mass dominated, when buoyancy forces are cooperating or opposing. We also note that this work is an extension and a further exploration of our previous studies, where we have considered an opposing flow in air-H_2O mixture only [26] or a cooperating flow in gas mixtures (air-CO_2 or air-H_2O) at two average concentrations of pollutant only (10% and 25%) [25].

2. Analysis and Modeling

2.1. Physical Model. The studied physical system is represented in Figure 1. It consists of a square cavity of width L, filled with air-CO_2 at different average concentration in CO_2. The vertical walls of the cavity are black and maintained at constant temperatures ($T_H > T_C$) and concentrations ($C_L < C_H$). These conditions are disposed so as to create an opposing or cooperating fluid flow. The horizontal walls are adiabatic, impermeable, and completely reflecting. The mixture density at the cold and hot walls, in the most severe conditions investigated here (20% CO_2), is, respectively, 0.80 kg/m^3 and 0.61 kg/m^3 in cooperating flow and 0.66 kg/m^3 and 0.73 kg/m^3 in opposing flow. So, from these values, we can note that the maximum density variations within the fluid are of order of 14% (cooperating flow-cold wall) if related to the reference value (0.70 kg/m^3) calculated at the average temperature ($T_0 = (T_H + T_C)/2$) and concentration ($C_0 = (C_H + C_L)/2$). Therefore, we have considered that the Boussinesq approximation remains valid within the frame of our study.

2.2. Governing Equations. The flow is assumed to be two-dimensional, stationary, and laminar. The fluid in the cavity is a mixture of pure air (considered as perfectly transparent) and CO_2 (an absorbing, emitting, and nonscattering species) acting as a pollutant. It is assumed Newtonian, incompressible, with constant thermophysical properties—except in the buoyancy term of the momentum equation—and satisfying the Boussinesq approximation. Under these assumptions, the fluid motion is described by the following set of equations, expressed in the vorticity (ω)-stream function (ψ) form:

$$\frac{\partial \omega}{\partial t} + u\frac{\partial \omega}{\partial x} + v\frac{\partial \omega}{\partial y} = \mathscr{V}\left(\frac{\partial^2 \omega}{\partial x^2} + \frac{\partial^2 \omega}{\partial y^2}\right) + g\left(\beta_T \frac{\partial T}{\partial x} + \beta_C \frac{\partial C}{\partial x}\right), \quad (1)$$

$$\frac{\partial T}{\partial t} + u\frac{\partial T}{\partial x} + v\frac{\partial T}{\partial y} = \alpha\left(\frac{\partial^2 T}{\partial x^2} + \frac{\partial^2 T}{\partial y^2}\right) + S_R, \quad (2)$$

$$\frac{\partial C}{\partial t} + u\frac{\partial C}{\partial x} + v\frac{\partial C}{\partial y} = D\left(\frac{\partial^2 C}{\partial x^2} + \frac{\partial^2 C}{\partial y^2}\right), \quad (3)$$

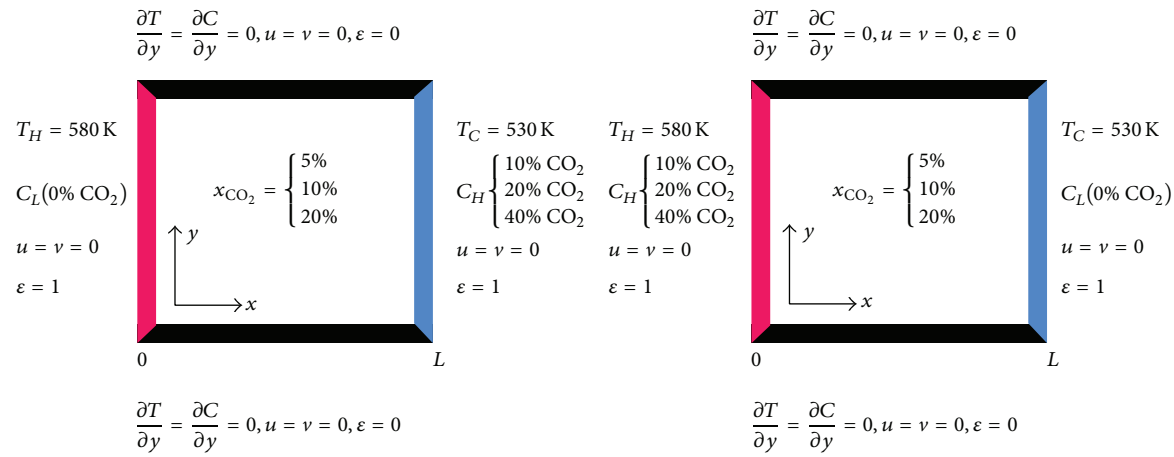

Figure 1: Physical model: (a) cooperating flow, (b) opposing flow.

$$-\omega = \frac{\partial^2 \psi}{\partial x^2} + \frac{\partial^2 \psi}{\partial y^2}, \tag{4}$$

$$u = \frac{\partial \psi}{\partial y}, \qquad v = -\frac{\partial \psi}{\partial x}, \tag{5}$$

where β_T and β_C are the thermal and mass expansion coefficients, respectively, defined by

$$\beta_T = -\frac{1}{\rho}\left(\frac{\partial \rho}{\partial T}\right)_{p,c} = \frac{1}{T_0},$$
$$\beta_C = -\frac{1}{\rho}\left(\frac{\partial \rho}{\partial C}\right)_{p,T} = \frac{M_{\text{air}} - M_{CO_2}}{\rho_0}. \tag{6}$$

M_{air} and M_{CO_2} are the molecular masses of air and CO_2.

In the energy equation (2), S_R stands for the radiation source field. It is calculated as explained below.

2.3. Radiation Model. The general equation for radiative transfer in an absorbing emitting medium is, in the (x, y) Cartesian coordinate frame,

$$\mu \frac{\partial I(x, y, s)}{\partial x} + \eta \frac{\partial I(x, y, s)}{\partial y} + \kappa(x, y) I(x, y, s) = \kappa(x, y) I_b(x, y). \tag{7}$$

I is the spectral radiation intensity in the direction s, κ represents the local spectral absorption coefficient, and I_b stands for the spectral blackbody intensity at local temperature. The absorption coefficient is directly linked to the concentration of pollutant since

$$\kappa(x, y) = C_{\text{abs}} \times C(x, y), \tag{8}$$

where C_{abs} is the spectral absorption cross-section of the considered species, evaluated at the local thermodynamic conditions (pressure, temperature).

In this paper, the discrete ordinate method (DOM), together with the SLW model of Denison and Webb [28], is used to solve the radiative transfer equation (RTE) and get the radiative fluxes and sources within the medium. The DOM is based on the selection of N_d discrete directions s_m to account for the directional dependence of the radiation intensity. The SLW model aims at representing the spectral radiative properties of the medium in a global yet accurate manner. It consists in replacing the real gas by a sum of N_g gray gases, each of them being associated with a given value of the absorption cross-section, C_{abs_k}, and a blackbody factor a_k which transforms the gas emission term into $I_{b,k} = a_k \sigma T^4/\pi$. Index k varies from 0 to N_g with, conventionally, $C_{\text{abs}_0} = 0$. Then the RTE is solved, for each gray gas k and each discrete direction m, as

$$\mu_m \frac{\partial I_{k,m}(x, y)}{\partial x} + \eta_m \frac{\partial I_{k,m}(x, y)}{\partial y} + \kappa_k(x, y) I_{k,m}(x, y) = \kappa_k(x, y) a_k \frac{\sigma T^4(x, y)}{\pi}, \tag{9}$$

where $I_{k,m}(x, y)$ is a shorthand for $I_k(x, y, s_m)$ and

$$\kappa_k(x, y) = C_{\text{abs}_k} \times C(x, y). \tag{10}$$

The values of a_k and C_{abs_k} vary in the medium with the local temperature and concentration (we assume atmospheric pressure everywhere). The a_k's are deduced from the closed-form functions of the reordered wave number developed by Denison and Webb [28, 29].

Table 1: Boundary conditions of the problem.

Wall	Temperature	Concentration		Stream function	Vorticity
		Cooperating case	Opposing case		
1 ($x = 0$)	T_H	C_L	C_H	$\psi = 0$	$\omega = -\partial^2\psi/\partial x^2$
2 ($x = L$)	T_C	C_H	C_L	$\psi = 0$	$\omega = -\partial^2\psi/\partial x^2$
3 ($y = 0$)	$q_t = 0$	$\partial C/\partial y = 0$		$\psi = 0$	$\omega = -\partial^2\psi/\partial y^2$
4 ($y = L$)	$q_t = 0$	$\partial C/\partial y = 0$		$\psi = 0$	$\omega = -\partial^2\psi/\partial y^2$

When using both the DOM and the SLW model, the incident fluxes at the walls are given by

$$q^{\text{inc}}_{x,k}(0,y) = \sum_{\mu_m<0} |\mu_m| w_m I_{k,m}(0,y),$$
$$q^{\text{inc}}_{x,k}(L,y) = \sum_{\mu_m>0} \mu_m w_m I_{k,m}(L,y), \tag{11a}$$
$$q^{\text{inc}}_{y,k}(x,0) = \sum_{\eta_m<0} |\eta_m| w_m I_{k,m}(x,0),$$
$$q^{\text{inc}}_{y,k}(x,L) = \sum_{\eta_m>0} \eta_m w_m I_{k,m}(x,L), \tag{11b}$$

where w_m is the weighting coefficient of direction m in the quadrature set. Equations (11a) apply to the vertical (active) walls while (11b) are for the horizontal (passive) ones. More generally, the x- and y-components of the total radiative flux at any point in the medium are

$$q_{R,x}(x,y) = \sum_{k=1}^{N_g}\sum_{m=1}^{N_d} \mu_m w_m I_{k,m}(x,y),$$
$$q_{R,y}(x,y) = \sum_{k=1}^{N_g}\sum_{m=1}^{N_d} \eta_m w_m I_{k,m}(x,y), \tag{12}$$

and the radiation source field (to be input in the energy equation) is obtained as

$$S_R(x,y) = \sum_{k=1}^{N_g} \kappa_k(x,y)\left(\sum_{m=1}^{N_d} w_m I_{k,m}(x,y) - 4a_k\sigma T^4(x,y)\right). \tag{13}$$

2.4. Initial and Boundary Conditions. Initially, the fluid is motionless, isothermal, and homogeneous at average temperature T_0 and average concentration C_0. The thermal, mass, and dynamic boundary conditions of the problem are summarized in Table 1. It should be noted that, to create a cooperating double diffusive flow (i.e., thermal and mass buoyancy forces augment each other), we impose at the hot wall the lowest concentration (C_L) of CO_2 (pollutant heavier than air) and the highest concentration (C_H) at the cold wall. For an opposing double diffusive flow, we must reverse (compared to cooperating case) these mass boundary conditions (C_H at hot wall and C_L at cold wall).

Regarding the radiative part of the problem, intensities leaving the vertical (black) walls correspond to the blackbody emission at the wall temperature:

$$I_{k,m}(0,y) = a_k\frac{\sigma T_H^4}{\pi} \quad \text{for } \mu_m > 0,$$
$$I_{k,m}(L,y) = a_k\frac{\sigma T_C^4}{\pi} \quad \text{for } \mu_m < 0, \tag{14a}$$

while the horizontal walls are assumed to be perfectly diffusively reflecting:

$$I_{k,m}(x,0) = \frac{q^{\text{inc}}_{y,k}(x,0)}{\pi} \quad \text{for } \eta_m > 0,$$
$$I_{k,m}(x,L) = \frac{q^{\text{inc}}_{y,k}(x,L)}{\pi} \quad \text{for } \eta_m < 0. \tag{14b}$$

2.5. Heat and Mass Transfer. The average Nusselt numbers (convective, radiative, and total) and Sherwood numbers at vertical walls are defined as follows:

$$\overline{\text{Nu}}_c = \frac{1}{(T_H - T_C)}\int_0^L \left|\frac{\partial T}{\partial x}\right|_{x=0 \text{ or } L} dy,$$
$$\overline{\text{Nu}}_R = \frac{1}{\lambda(T_H - T_C)}\int_0^L \left|q_R^{\text{net}}\right|_{x=0 \text{ or } L} dy, \tag{15}$$

where q_R^{net} represents the net radiative flux (emitted + absorbed) at vertical walls, given by

$$q_R^{\text{net}}\Big|_{x=0 \text{ or } L} = \varepsilon_p\left(\sigma T_w^4 - \sum_{k=1}^{N_g} q^{\text{inc}}_{x,k}\right)\Bigg|_{x=0 \text{ or } L},$$
$$\overline{\text{Nu}}_t = \overline{\text{Nu}}_c + \overline{\text{Nu}}_R, \tag{16}$$
$$\overline{\text{Sh}} = \frac{1}{(C_H - C_L)}\int_0^L \left|\frac{\partial C}{\partial x}\right|_{x=0 \text{ or } L} dy.$$

3. Numerical Procedure

The thermophysical properties of the mixture are calculated at T_0 and C_0 (reference state) according to the ideal gas

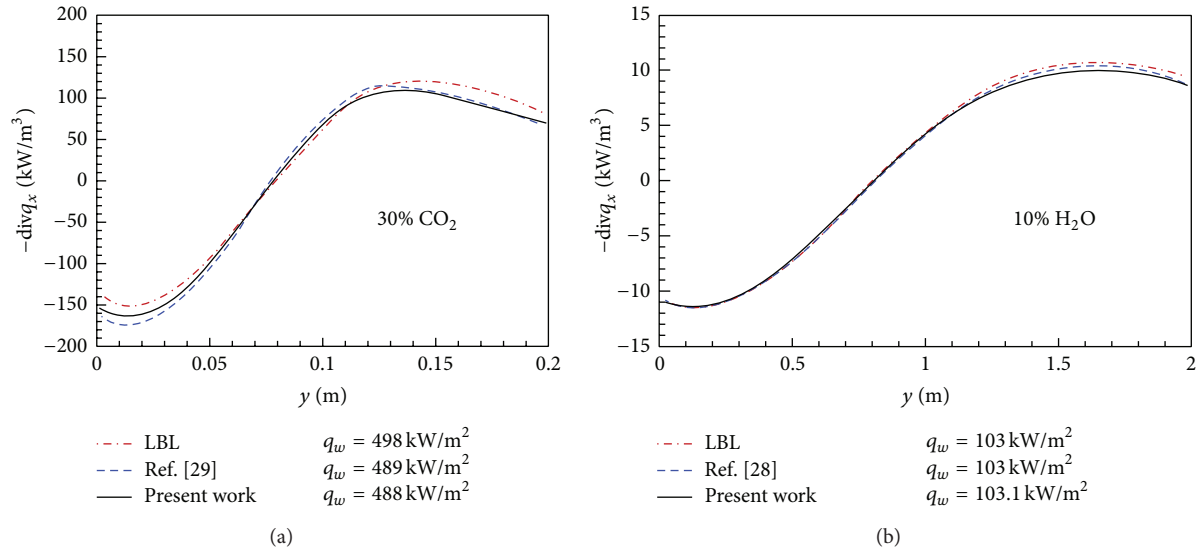

FIGURE 2: Radiative source and net cold wall: (a) fluid at 30% CO_2; $T_H - T_C = 1000$ K; $T_0 = 1250$ K; (b) fluid at 10% H_2O; $T_H - T_C = 500$ K; $T_0 = 1000$ K.

laws (for molecular mass and density), Wilke and Wassiljewa formulas (for dynamic viscosity and thermal conductivity), and the empirical relation of Fuller et al. [30] (for mass diffusivities of water vapour into air). Equations (1)–(3) are solved by a finite difference method based on an ADI scheme. The first and second space derivatives are approximated by central differences and the time derivatives by a first-order forward difference. The Poisson equation (4) is solved by the successive over relaxation method. A nonuniform grid (80 × 80) with hyperbolic tangent distribution in x- and y-direction is used herein:

$$x_i = 0.5\left[1 + \frac{\text{th}\left(\delta\left(i/80 - 0.5\right)\right)}{\text{th}\left(\delta/2\right)}\right],$$
$$y_i = 0.5\left[1 + \frac{\text{th}\left(\delta\left(j/80 - 0.5\right)\right)}{\text{th}\left(\delta/2\right)}\right], \quad (17)$$

where δ is a stretching parameter, set to 4 in this study.

All the calculations are performed using a false transient method. A steady state solution is assumed to be reached when the two following criteria are met:

$$\left|\frac{f_{i,j}^{n+1} - f_{i,j}^{n}}{f_{i,j}^{n+1}}\right| \le 10^{-4}, \quad (18)$$

$$\left|\frac{\left(\overline{\text{Nu}}_t, \overline{\text{Sh}}\right)_{x=0} - \left(\overline{\text{Nu}}_t, \overline{\text{Sh}}\right)_{x=L}}{\left(\left(\overline{\text{Nu}}_t, \overline{\text{Sh}}\right)_{x=0} + \left(\overline{\text{Nu}}_t, \overline{\text{Sh}}\right)_{x=L}\right)/2}\right| \le 10^{-4}, \quad (19)$$

where f stands for T, C and ψ; n is the iteration number. The second constraint equation (19) ensures that, at steady state, the total heat and mass flux input to the cavity through one vertical wall must be equal to those leaving the other.

3.1. Validation of the Computer Code. The accuracy of the numerical results was checked through several tests based on the effects of grid size (Table 2) and number of gray gases N_g (Table 3) required to characterize the radiative properties of the fluid (SLW model). For this, we consider a square cavity filled with a mixture at 10% CO_2 and submitted to the same boundary conditions as shown in Figure 1(a). It can be seen that an 80 × 80 grid and $N_g = 11$ gray gases for the SLW model (one of them being transparent) are sufficient to ensure a relative accuracy of order 0.1%. This conclusion was found to remain valid with other concentrations of CO_2.

The predictions of our model were also successfully validated against previously published results in different situations. First, in double diffusive convection, the average Nusselt and Sherwood numbers (Table 4) agree within a maximum relative error of 0,44% with that obtained by Béghein et al. [31]. Dealing with convection in gray fluid (Table 5), we note a maximum discrepancy of 0,3% on the radiative Nusselt number and of 0,54% on the total Nusselt

TABLE 2: Grid size effect on the average Nusselt (convective and total) and Sherwood numbers.

Grid size	$\overline{\text{Nu}}_c$	$\overline{\text{Nu}}_t$	$\overline{\text{Sh}}$
40 × 40	15,819	198,486	21,431
80 × 80	15,970	198,564	21,444
160 × 160	15,968	198,562	21,445

TABLE 3: Effect of the number of gray gases on the average Nusselt (convective and total) and Sherwood numbers.

Number of gray gases	$\overline{\text{Nu}}_c$		$\overline{\text{Nu}}_t$	$\overline{\text{Sh}}$
	Hot wall	Cold wall		
5	15,71	18,95	198,02	21,49
11	15,97	18,67	198,56	21,45
17	15,98	18,66	198,59	21,45

Table 4: Average convective Nusselt and Sherwood numbers: Ra = 10^7; Pr = 0,71; Le = 1.

	N	−0,01	−0,2	−0,5	−0,8	−1,5	−5
$\overline{\mathrm{Nu}}_C$ ($\overline{\mathrm{Sh}}$)	Present work (80 × 80)	16,40	15,49	13,65	10,64	13,66	23,77
		−16,40	−15,49	−13,65	−10,64	−13,66	−23,77
	Béghein et al. [31] (45 × 45)	16,4	15,5	13,6	10,6	13,6	23,7
		−16,4	−15,5	−13,6	−10,6	−13,6	−23,7

Table 5: Average Nusselt (radiative and total) number for different opacity of a gray gas: Ra = 5 × 10^6; Pr = 0,71; Pl = 0,02; θ_0 = 1,5.

τ	S_N	Present work (80 × 80)		Yucel et al. [8] (50 × 50)	
		$\overline{\mathrm{Nu}}_r$	$\overline{\mathrm{Nu}}_t$	$\overline{\mathrm{Nu}}_r$	$\overline{\mathrm{Nu}}_t$
1	S_8	31,25	38,81	31,28	38,93
5	S_4	23,57	31,59	23,64	31,76
0,2	S_4	37,40	46,05	37,40	46,11

Table 6: Dimensionless numbers corresponding to cooperating and opposing flow.

Pollutant	x (%)	N	Ra	Pr	Pl	Le
CO_2	5	±0,57	$8{,}85 \times 10^6$	0,72	$3{,}58 \times 10^{-3}$	1,30
	10	±1,10	$9{,}44 \times 10^6$	0,72	$3{,}55 \times 10^{-3}$	1,26
	20	±2,10	$1{,}09 \times 10^7$	0,72	$3{,}50 \times 10^{-3}$	1,18

number when comparing to [8] (the maximum error is reached when the medium optical thickness is about 5). In the case of nongray gas radiation, the average total Nusselt number obtained compared well with Fusegi's data (laminar flow, L = 7,62 cm, relative error 0,85%) [13]. Finally, The accuracy of the SLW spectral model (Figure 2) was more particularly assessed by comparison to [28, 29]. For this test we considered a homogenous and nonisothermal fluid, with a cosine temperature distribution $T(x) = T_0 + 0.5(T_H - T_C)\cos(\pi x/L)$, placed between infinite parallel black walls ($\varepsilon_p = 1$) maintained at T_H and T_C.

4. Results and Discussion

4.1. Conditions of Simulations. The results presented in this investigation were obtained by considering the following parameters: L = 0.3 m, T_H = 580 K, and T_C = 530 K. In cooperating flow (i.e., where thermal and mass buoyancy forces augment each other), a null concentration of CO_2 is prescribed at the hot wall (C_L = 0 mol/m^3 or x_L = 0%) and, at the cold wall, the concentration is set to C_H = 2.20, 4.39, and 8.78 mol/m^3. These correspond, respectively, in reference conditions, to molar fractions x_{CO_2} = 10%, 20%, and 40%. Now, to create an opposing double diffusive flow (i.e., thermal and mass buoyancy forces are opposite), the mass boundary conditions must be reversed: C_L at the cold wall and C_H at the hot wall.

In the SLW model, the reference state values of temperature and molar fraction were T_0 = 555 K and the average molar fractions x_{CO_2} = 5%, 10%, and 20%. Based on these data, the mass-to-thermal buoyancy ratio (N), thermal Rayleigh number (Ra), Prandtl (Pr), Planck (Pl), and Lewis number (Le) relating to the problem are summarized in Table 6. Values of $|N|$ below unity (0.57) characterize a flow mainly driven by thermal forces (thermal regime), whereas values above unity (2.10) refer to a flow dominated by concentration gradients (mass regime). In between ($|N|$ = 1.10) mass and thermal effects are of comparable magnitude (intermediate regime).

It is worth noting that the effects of gas radiation on field characteristics were determined by comparison to the nonparticipating gas case (i.e., a fluid having the same thermophysical properties as the considered mixtures, but totally transparent).

4.2. Flow Patterns

4.2.1. Cooperating Flow. Figures 3 and 4 display the streamline, temperature, and concentration contours for different average molar fractions of CO_2 in the cavity (x_{CO_2} = 5%, 10%, and 20%), when the gas is transparent or participating to radiation. On the whole, we can see (Figure 4(a)) that, when the buoyancy forces (mass and thermal) are cooperating, gas radiation weakly alters the flow pattern (slight slope and distortion of the streamlines, small secondary cells in the core of cavity). These modifications are less important at 20% CO_2 than at 5% (and 10%), because a higher rate of absorbing species strengthens the mass forces and increases buoyancy ratio (N) from 0,57 to 2,10 (see Table 6). This makes the flow mainly driven by concentration (not temperature) gradients and hence less sensitive to radiation. Under gas radiation effects, the vertical boundary layers are broadened and partially accelerated (Figures 5(c) and 5(d)), whereas the core of the cavity is unaffected and remains at rest. This induces an increase of horizontal jets flowing from one active wall to the other along the adiabatic surfaces (Figures 5(a) and 5(b)). The strengthening of the vertical boundary layers, associated with fixed concentrations at vertical walls, leads to an excess of pollutant (CO_2) near the left wall (at C_H) and a deficit near the right one (at C_L) (Figure 6(a)). To equilibrate this trend, some part of CO_2 is diffused from left to right, resulting in negative gradient of concentration in the x-direction. This breaks the centrosymmetry of the field and replaces the vertical stratification by a tilted iso-concentration pattern (Figure 4(b)) [25].

Regarding the thermal field, the gas flowing under the upper wall emits radiation. It is slightly colder than it would be without radiative effects (Figure 6(b), air-CO_2 mixture, y/L = 0.875), and this weakens the temperature gradient at vertical cold wall when the fluid flows downward. A

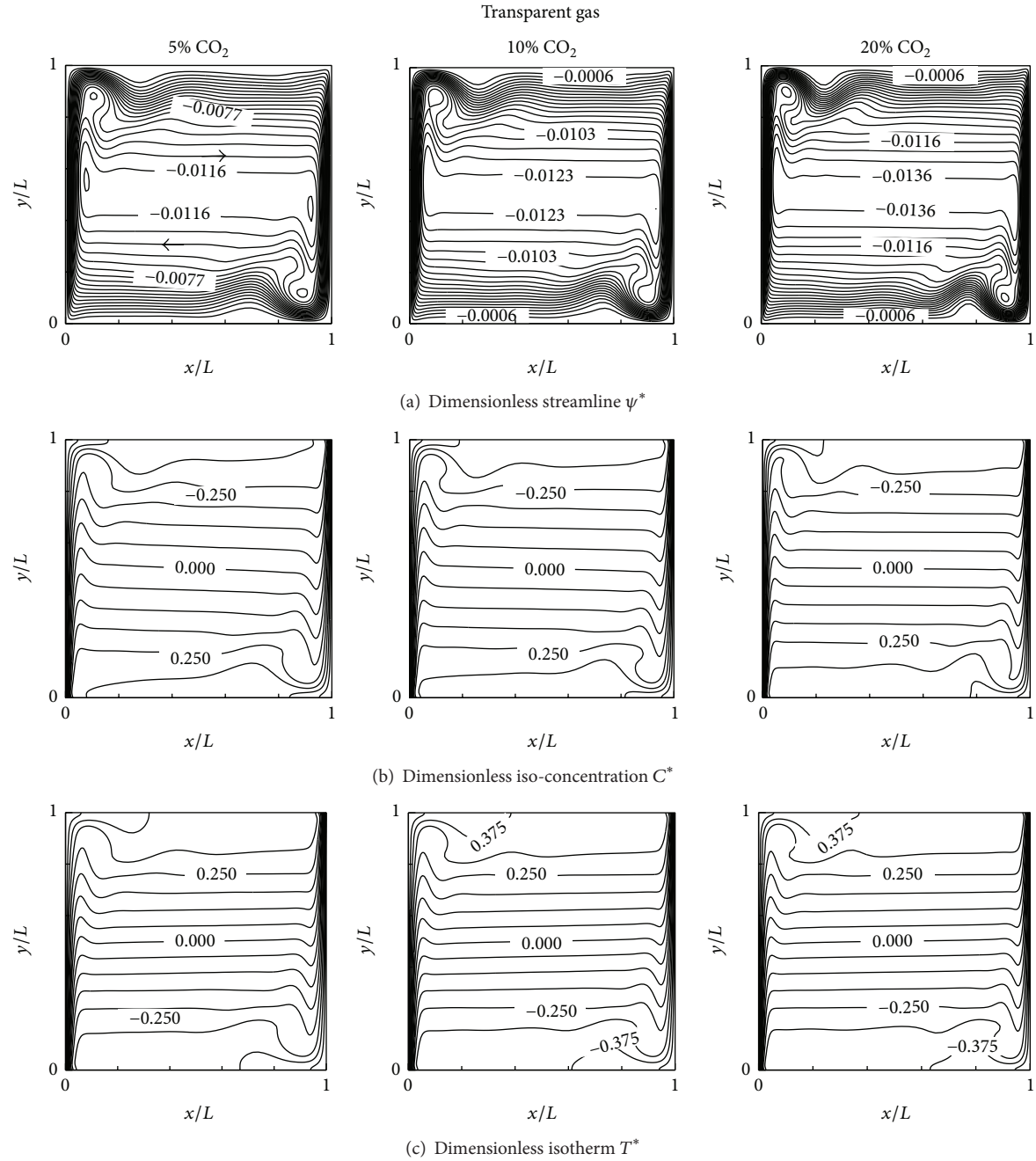

(a) Dimensionless streamline ψ^*

(b) Dimensionless iso-concentration C^*

(c) Dimensionless isotherm T^*

FIGURE 3: Dimensionless streamline, iso-concentration, and isotherm patterns for air-CO_2 mixture at 5%, 10%, and 20% CO_2, in cooperating flow. (a) $\psi^* = \psi\sqrt{g\beta_T(T_H - T_C)L^3}$, $\Delta\psi^* = 0.00065$; (b) $C^* = (C - C_0)/(C_H - C_L)$, $\Delta C^* = 0.0625$; (c) $T^* = (T - T_0)/(T_H - T_C)$, $\Delta T^* = 0.0625$.

symmetrical picture is observed along the bottom wall (Figure 6(b), air-CO_2 mixture, $y/L = 0.125$) where the fluid is preheated by absorbing radiation, leading to a reduction of the temperature gradient along the vertical hot wall. In the core of the cavity (outside boundary layers) (Figure 6(b), air-CO_2, $y/L = 0.5$), while the reference transparent gas remains practically isothermal, the gas is heated by absorption of radiation from the hot wall in the left part of the cavity and is cooled by emission toward the cold wall in the right part. As a result (in the center of the cavity) negative temperature gradients in the x-direction are formed and will create a thermal field with tilted stratification (Figure 4(c)). This trend is more pronounced at 20% CO_2 than at 10% and 5%.

4.2.2. Opposing Case. For an average concentration of 5% of CO_2, the fluid flow in the cavity is mainly driven by thermal forces if gas absorption is neglected (Figure 7(a), 5% CO_2). When taken into account (Figure 8(a), 5% CO_2),

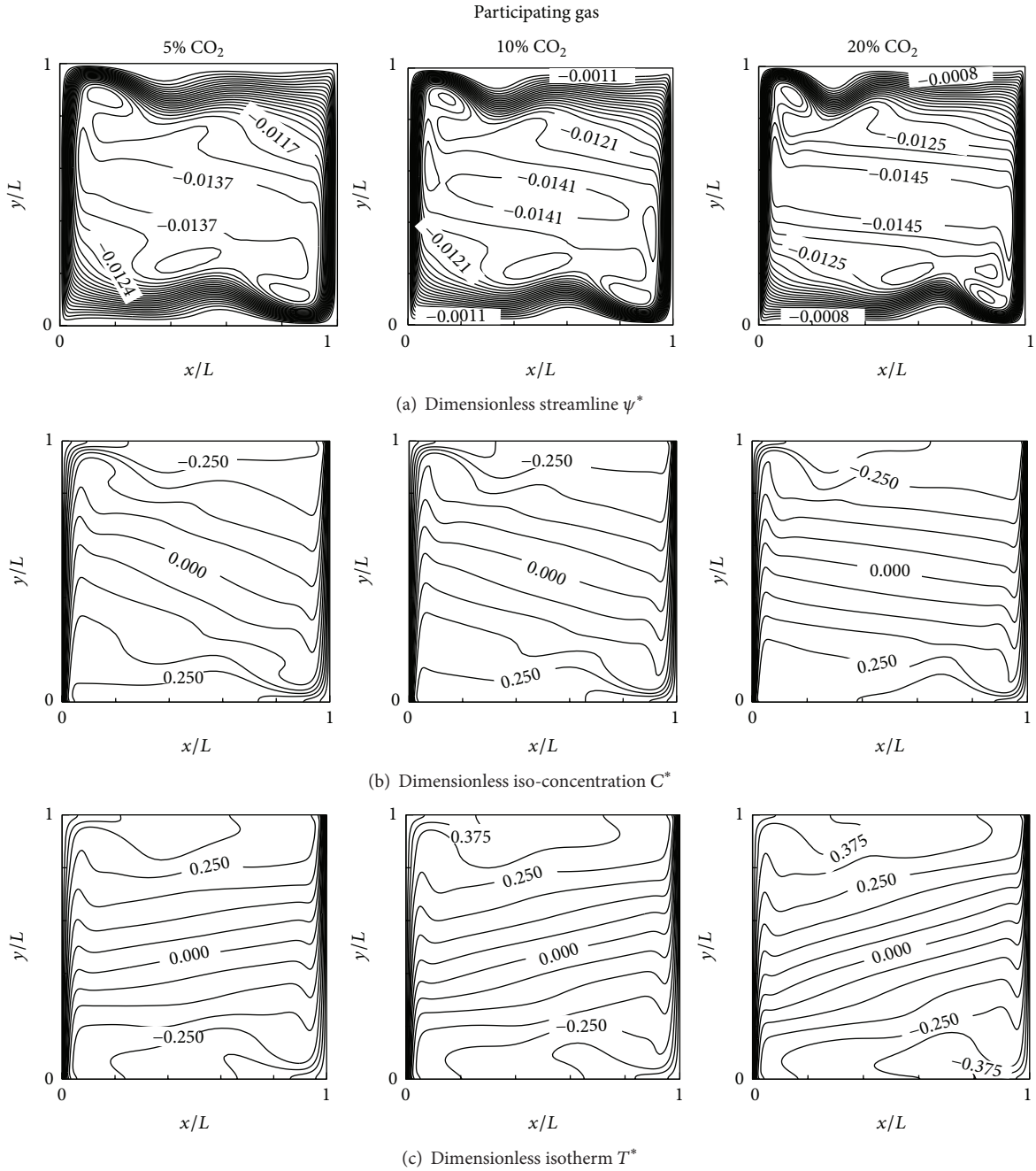

(a) Dimensionless streamline ψ^*

(b) Dimensionless iso-concentration C^*

(c) Dimensionless isotherm T^*

FIGURE 4: Dimensionless streamline, iso-concentration, and isotherm patterns for air-CO_2 mixture at 5%, 10%, and 20% CO_2, in cooperating flow. (a) $\psi^* = \psi\sqrt{g\beta_T(T_H - T_C)L^3}$, $\Delta\psi^* = 0.00065$; (b) $C^* = (C - C_0)/(C_H - C_L)$, $\Delta C^* = 0.0625$; (c) $T^* = (T - T_0)/(T_H - T_C)$, $\Delta T^* = 0.0625$.

radiation accelerates boundary layers (Figure 9(b), 5% CO_2) by enhancing the thermal forces near the horizontals walls (as in cooperating case). The stagnant core of the cavity (for transparent gas) is also set in motion (thermal forces are slightly weakened). Such behavior tends to homogenize the concentration and temperature fields, whose stratifications are destroyed (Figure 8(b), 5% CO_2). In this case (at 5% CO_2), the magnitude of radiation effects on the structure of the different fields seems to be greater in opposing flow than in cooperating case, indicating that a lower flow dynamics when the thermal and mass buoyancy forces are opposing (equivalent Rayleigh number: $|N + 1|$Ra lower) promotes the influence of radiation.

Independently of gas radiation, the increase in concentration of pollutant (to 10% CO_2) slightly strengthens the mass forces, which become comparable to the thermal ones. In this configuration, a multicellular flow structure is observed (transitional flow) (Figure 7(a), 10% CO_2): two

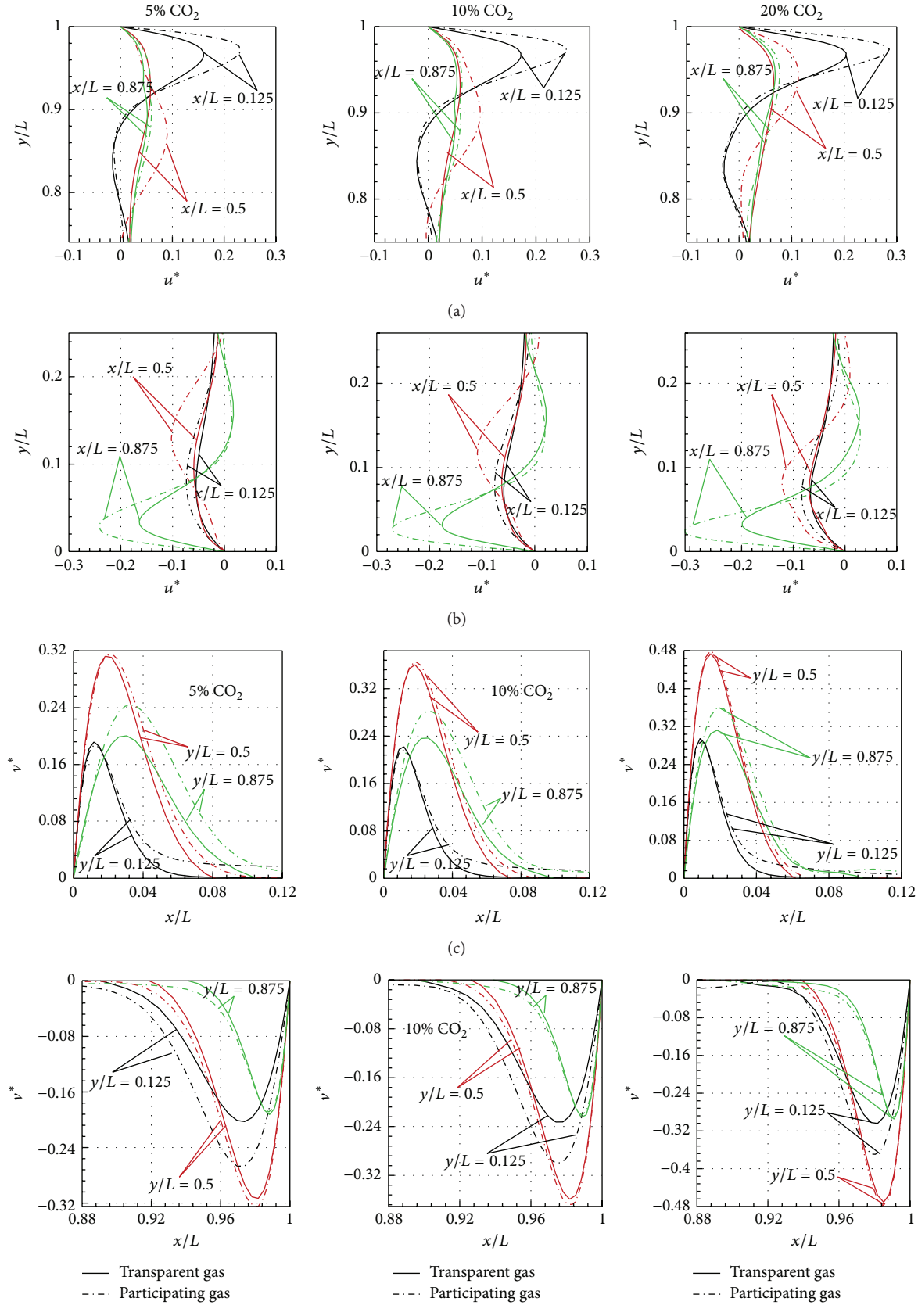

FIGURE 5: Dimensionless vertical and horizontal velocity at different levels in the cavity, for cooperating flow: air-CO_2 mixtures at 5%, 10%, and 20% CO_2. $v^* = v(g\beta_T(T_H - T_C)L)^{-0.5}$, $u^* = u(g\beta_T(T_H - T_C)L)^{-0.5}$. (a) Upper wall, (b) lower wall, (c) hot wall, and (d) cold wall.

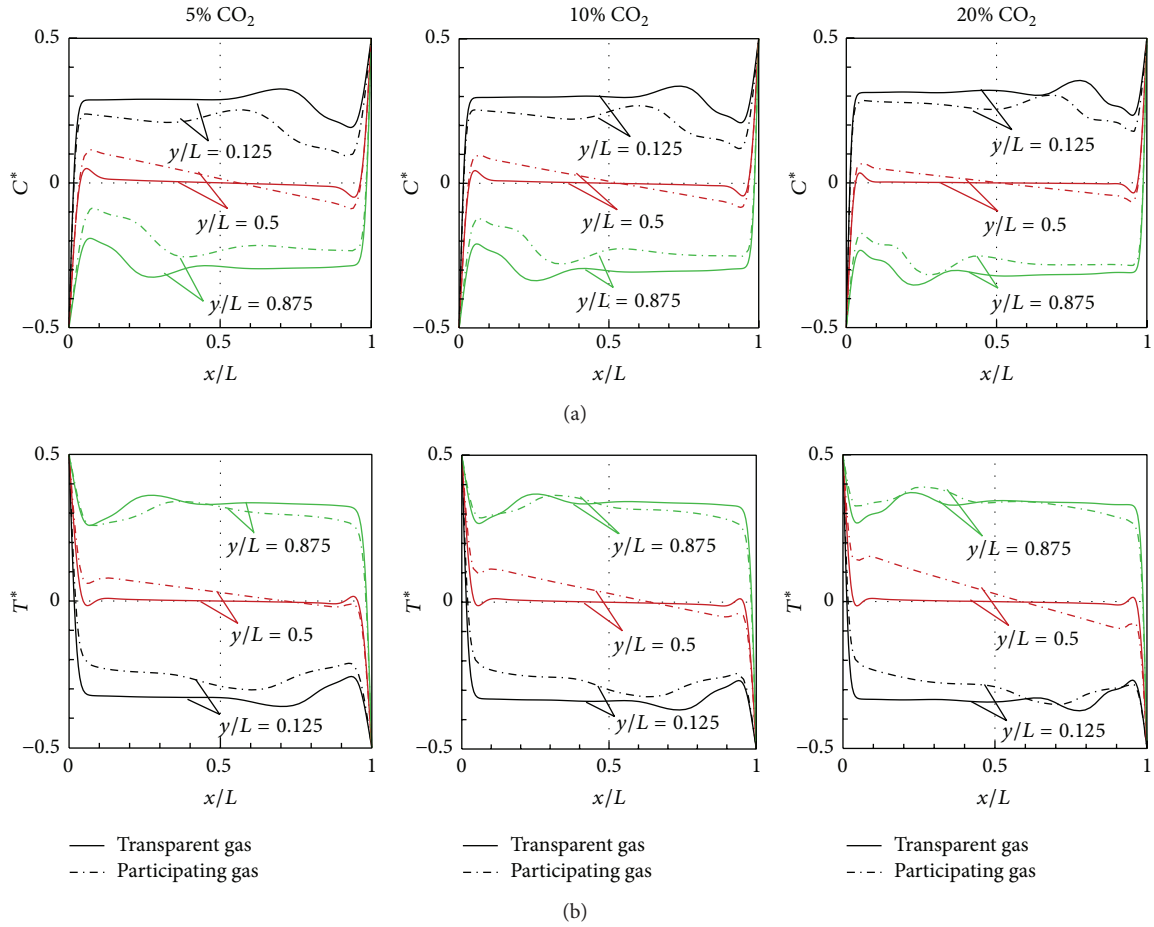

FIGURE 6: Dimensionless concentration (a) and temperature (b) profiles at different heights in the cavity, for a cooperating flow. $C^* = (C - C_0)/(C_H - C_L)$, $T^* = (T - T_0)/(T_H - T_C)$.

cells of thermal origin near the horizontal walls and one cell of mass origin in the center of cavity. Under radiation effect, the horizontal temperature gradients, at the vicinity of the horizontals walls (where thermal forces are dominant even with transparent gas), are enhanced. This accelerates the flow in thermal cells (upper and lower) and consequently in mass cell as well (Figure 9(b), 10% CO_2). Radiation does not practically alter the structure of the concentration field (since the flow dynamics which controls the mass transfer itself is unaffected). However, we note a decrease in pollutant concentration at the top and center of the cavity and an increase at the bottom (Figure 10(a), $y/L = 0.875$ and 0.125), due to acceleration of the fluid within cells. The structure of the thermal field is also little affected by radiation (Figure 8(c), 10% CO_2). Also, a warming of the fluid can be noted in the upper part of the cavity and its cooling in the center and in the lower part (Figure 10(b), $y/L = 0.875$ and 0.125). This causes (in association with the fluid flow direction) an increase of the temperature gradients along the vertical walls.

For mixture at 20% CO_2, when the gas is transparent, the fluid dynamics is dominated by mass buoyancy forces (mass flow regime) with a monocellular flow in anticlockwise direction (Figure 7(a), 20% CO_2). Under gas radiation effect, thermal forces are strengthened near the horizontal walls. As these two types of forces are present in opposing flow, dominated by mass forces, their resultant is reduced, yielding a slowdown (and even stop) of horizontal boundary layers. The vertical boundary layers are also slowed (partially) (Figure 9(b), 20% CO_2), which causes inclination of streamlines. But, owing to the strong dominance of mass forces ($N = -2.10$), the flow structure is globally maintained. Radiation causes the inclination of iso-concentrations and isotherms (i.e., formation of negative horizontal gradients of concentration and temperature) and a decrease of gradients of temperature at vertical walls: fluid warmer at hot wall and colder at the cold wall. These behaviors have also been observed in the cooperating case.

4.3. Heat and Mass Transfer

4.3.1. Cooperating Flow. The variation of average convective Nusselt number ($\overline{Nu}_c$), with pollutant (CO_2) concentration, at vertical walls is illustrated in Figure 11(a). It can be seen that radiation reduces the average convective flux because of

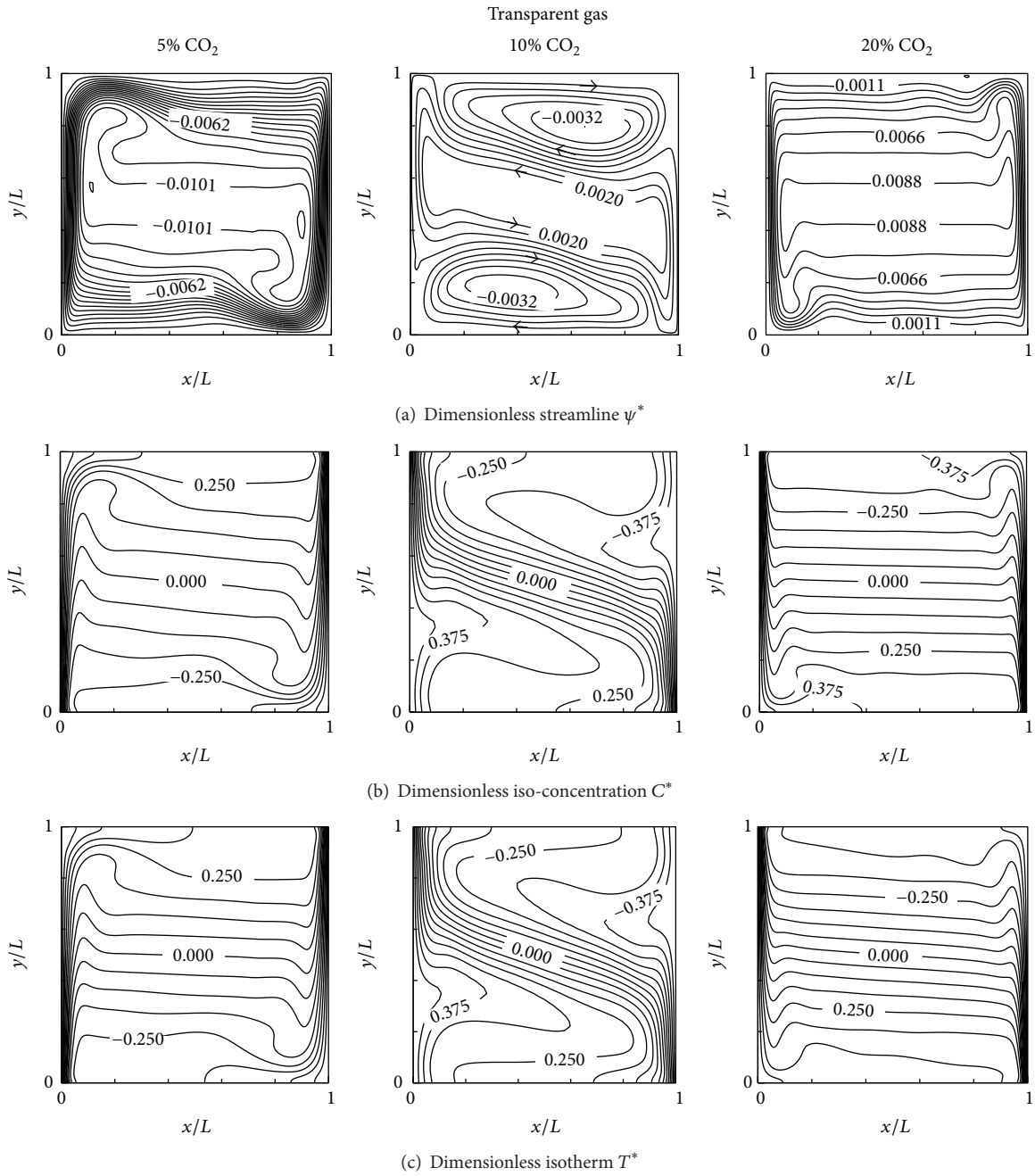

(a) Dimensionless streamline ψ^*

(b) Dimensionless iso-concentration C^*

(c) Dimensionless isotherm T^*

FIGURE 7: Dimensionless streamline, iso-concentration, and isotherm patterns for air-CO_2 mixture at 5%, 10%, and 20% CO_2, in opposing flow. (a) $\psi^* = \psi\sqrt{g\beta_T(T_H - T_C)L^3}$, $\Delta\psi^* = 0.00065$; (b) $C^* = (C - C_0)/(C_H - C_L)$, $\Delta C^* = 0.0625$; (c) $T^* = (T - T_0)/(T_H - T_C)$, $\Delta T^* = 0.0625$.

the weakening of the temperature gradient at vertical walls. The same trend is observed for the total Nusselt number (convective + radiative) (Figure 11(b)) due to the attenuation by the fluid of the radiative exchange between the active walls. This attenuation gets stronger when increasing concentration of absorbing species. It is worth noting that mass transfer (average Sherwood number $\overline{\mathrm{Sh}}$) is very weakly altered by gas radiation because it is primarily controlled by the flow dynamics, itself less sensitive to radiation than the thermal field (Figure 11(c)).

4.3.2. Opposing Flow. Contrarily to the cooperating case, when mass and thermal buoyancy forces are opposed (Figure 12(a)) different radiation effects can be observed on the average convective Nusselt number ($\overline{\mathrm{Nu}}_c$). This parameter is essentially reduced at high pollutant concentration corresponding to a mass flow regime and is less altered in thermal regime (reduction due to the weakening of temperature gradients at active walls) and transitional regime (augmentation due to acceleration of motion and increase of temperature gradients at active walls). The total Nusselt

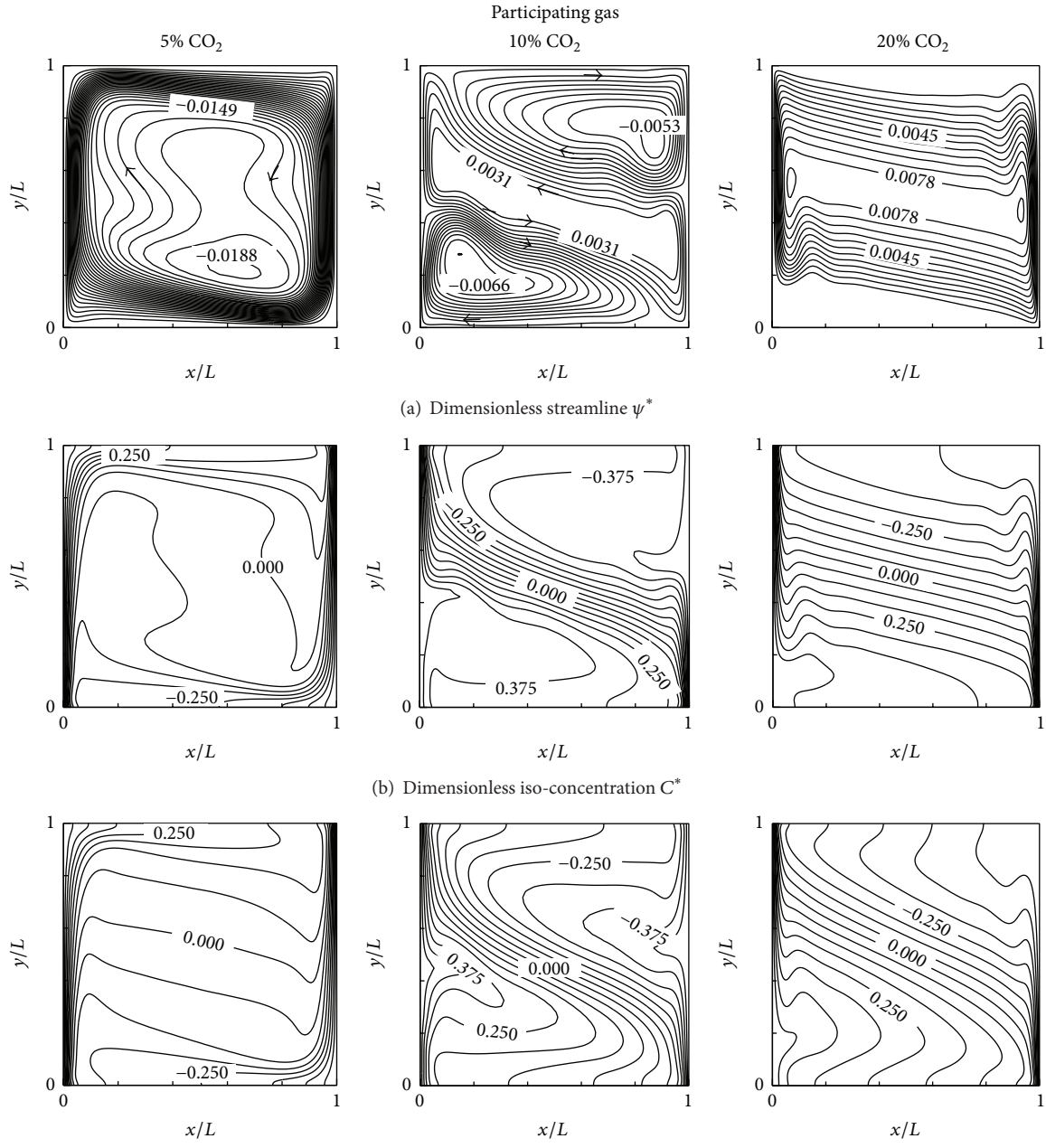

FIGURE 8: Dimensionless streamline, iso-concentration, and isotherm patterns for air-CO_2 mixture at 5%, 10%, and 20% CO_2, in opposing flow. (a) $\psi^* = \psi\sqrt{g\beta_T(T_H - T_C)L^3}$, $\Delta\psi^* = 0.00065$; (b) $C^* = (C - C_0)/(C_H - C_L)$, $\Delta C^* = 0.0625$; (c) $T^* = (T - T_0)/(T_H - T_C)$, $\Delta T^* = 0.0625$.

number (Figure 12(b)) is decreased whatever the concentration of pollutant is (so regardless the flow regime: thermal, transitional, or mass). Regarding mass transfer, outside the thermal regime, average mass flux ($\overline{\mathrm{Sh}}$) becomes a little more sensitive to gas radiation (than in the cooperating case) (Figure 12(c)): it is increased in transitional regime and reduced in mass regime.

5. Conclusions

In this work, we analyzed the effects of radiation of gas radiation on laminar double-diffusive convection in a nongray air-CO_2, when the thermal and mass buoyancy forces are cooperating or opposing. The real radiative participation of mixtures is accounted for by using the SLW spectral model of Denison and Webb. Three average concentrations of pollutants were considered so as to cover the different flow regimes: thermal (x_{CO_2} = 5%), transitional (10%), and mass (20%).

(i) In cooperating case, the results show that gas radiation has little influence on flow structure (only an acceleration of boundary layers and the core of the cavity remains practically at rest) but disturbs the

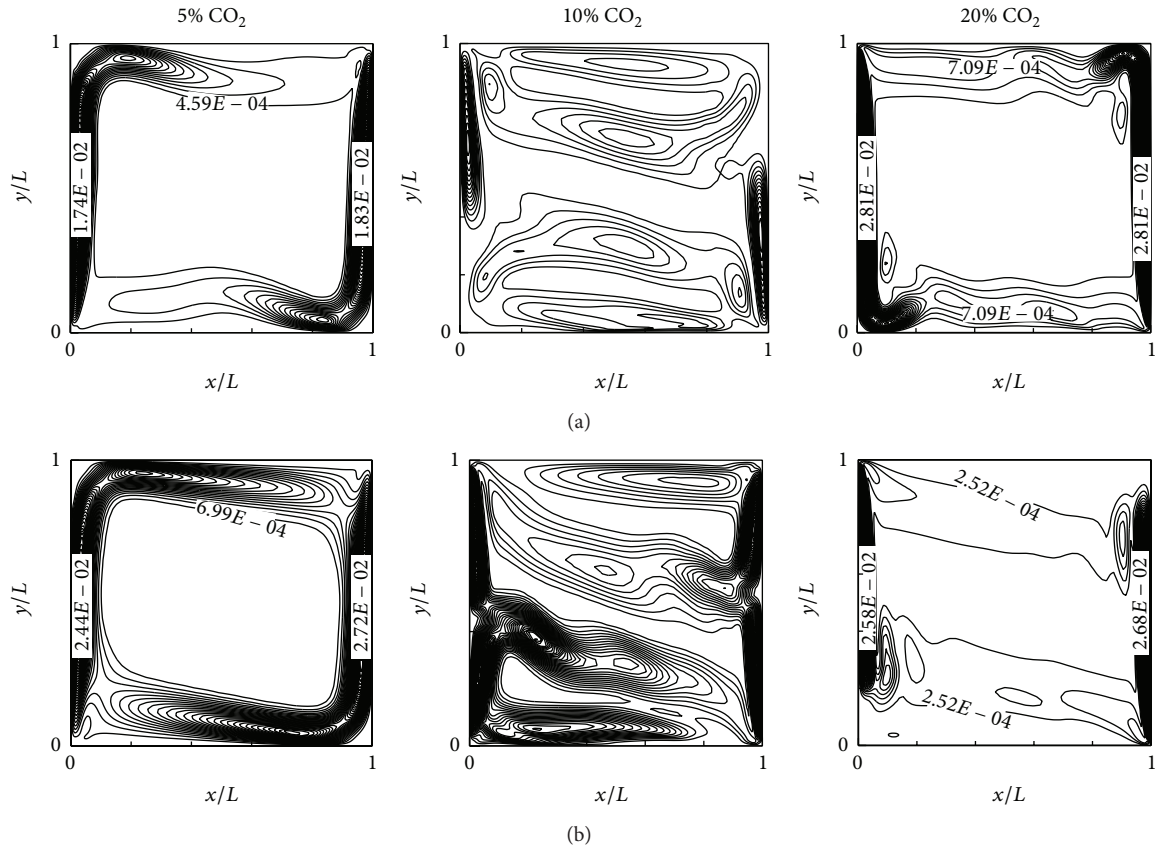

Figure 9: Dimensionless kinetic energy at different concentration of CO_2, in opposing flow: (a) transparent gas; (b) participating gas. $e_C^* = 0.5(u^2 + v^2)(g\beta_T(T_H - T_C)L)^{-1}$.

temperature and concentration fields, particularly by inclining their iso-values lines. The global heat transfer (total Nusselt number) is decreased, whereas the mass transfer (Sherwood numbers) is weakly affected (slightly decreased). These effects are observed for all considered concentrations (i.e., for all convective flow regimes).

(ii) In opposing case, radiation effects are more important than in cooperating flow and depend on the nature of the flow regime (in the absence of radiation):

(a) in thermal regime (x_{CO_2} = 5%): the fluid is accelerated across the cavity and this strongly alters the structure of the dynamic field and breaks the vertical stratification of temperature and concentration fields (essentially). Convective heat transfer is reduced by a decrease of the horizontal gradient of temperature at vertical walls;

(b) in transitional regime (x_{CO_2} = 10% CO_2): the fluid is also accelerated across the cavity without altering the structures of different fields. Convective heat transfer at vertical walls is increased (essentially at hot wall), by acceleration of the fluid flow and increase of the wall gradient of temperature;

(c) in mass regime (x_{CO_2} = 20%): the fluid is decelerated and gas radiation tends to replace the vertically stratified distribution of the temperature and concentration by a field with inclined iso-value lines (as in cooperating case). Average convective heat transfers are greatly reduced;

(d) more generally, gas radiation weakens the global heat transfer (conductive + radiative) whatever the flow regime is (as cooperating case) and also affects the mass transfer in transitional and mass regime.

Nomenclature

a: Weighting coefficient in the SLW model
C: Species concentration, mol/m^3
C_{abs}: Absorption cross-section, m^2/mol
D: Binary mass diffusion coefficient, m^2/s
g: Gravitational acceleration, m/s^2
I: Radiation intensity, W/m^2·sr or W/m^2·sr·μm
N: Mass-to-thermal buoyancy ratio = $\beta_C(C_H - C_L)/\beta_T(T_H - T_C)$
N_g: Number of gray gases
Nu: Nusselt number

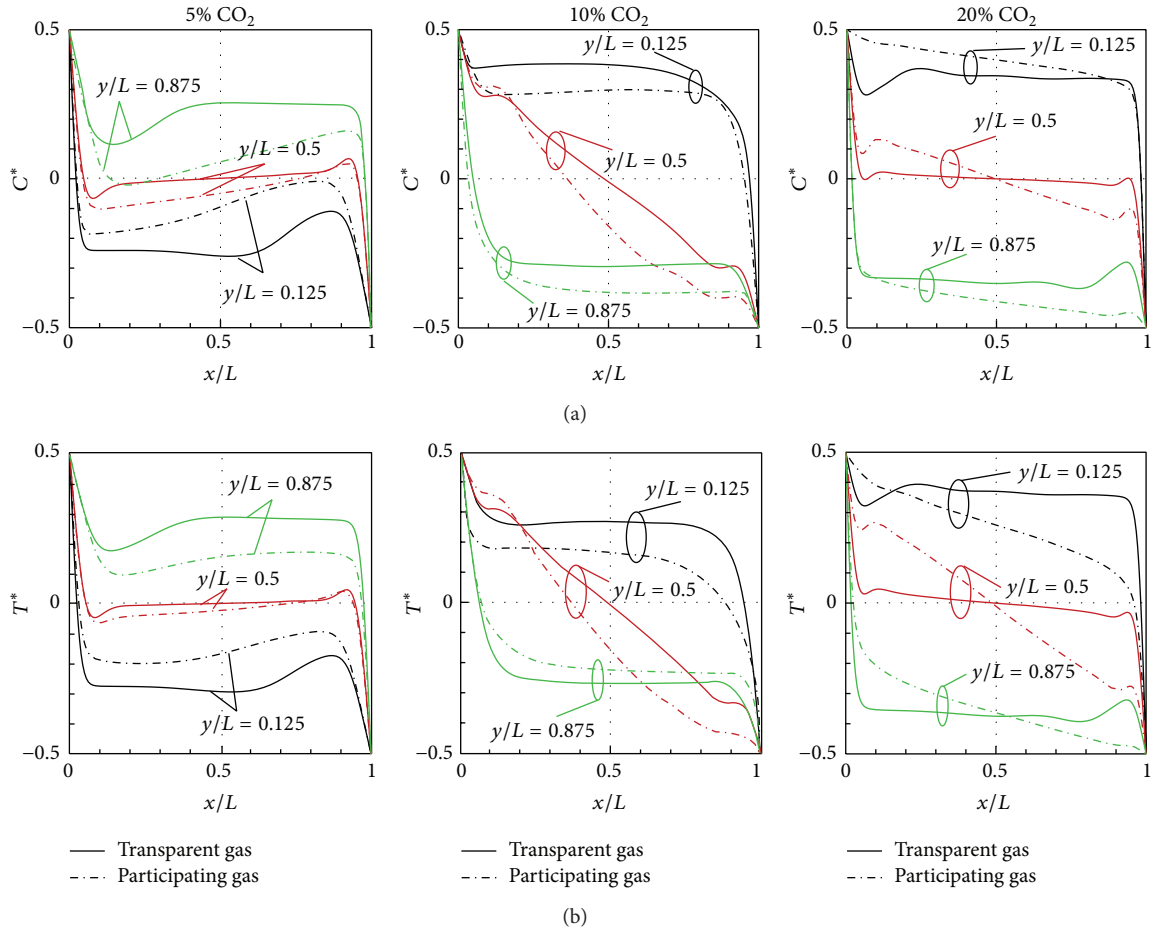

Figure 10: Dimensionless concentration (a) and temperature (b) profiles at different heights in the cavity, for an opposing flow: mixture at 5%, 10%, and 20% CO_2, $C^* = (C - C_0)/(C_H - C_L)$, $T^* = (T - T_0)/(T_H - T_C)$.

q^{inc}: Incident heat flux at wall, W/m^2
q_R: Radiative flux, W/m^2
s: Direction of radiation propagation
Sh: Sherwood number
S_R: Radiative source term, W/m^3
t: Time, s
T_w: Wall temperature, K
u, v: Horizontal and vertical velocities, m/s
w: Weight of angular quadrature
x, y: Spatial coordinates, m
x_{CO_2}: Average molar fraction of CO_2 at reference conditions
α: Mixture thermal diffusivity, m^2/s
β_T: Thermal expansion coefficient, 1/K
β_C: Mass expansion coefficient, m^3/mol
ε: Wall emissivity
κ: Absorption coefficient, 1/m
λ: Thermal conductivity, $W/m \cdot K$
μ, η: Direction cosines
$\mathcal{V}$: Mixture kinematic viscosity, m^2/s
ρ: Density, kg/m^3
σ: Stefan-Boltzmann constant, $W/m^2 \cdot K^4$
ω: Vorticity, 1/s
ψ: Stream function, m^2/s.

Subscript

C: Cold
c: Convective
H: Hot or high
k: kth gray gas
L: Low
m: mth direction of radiation propagation
R: Radiative quantity
x, y: In the x- or y-direction
0: Reference quantity.

Conflict of Interests

The authors declare that there is no conflict of interests regarding the publication of this paper.

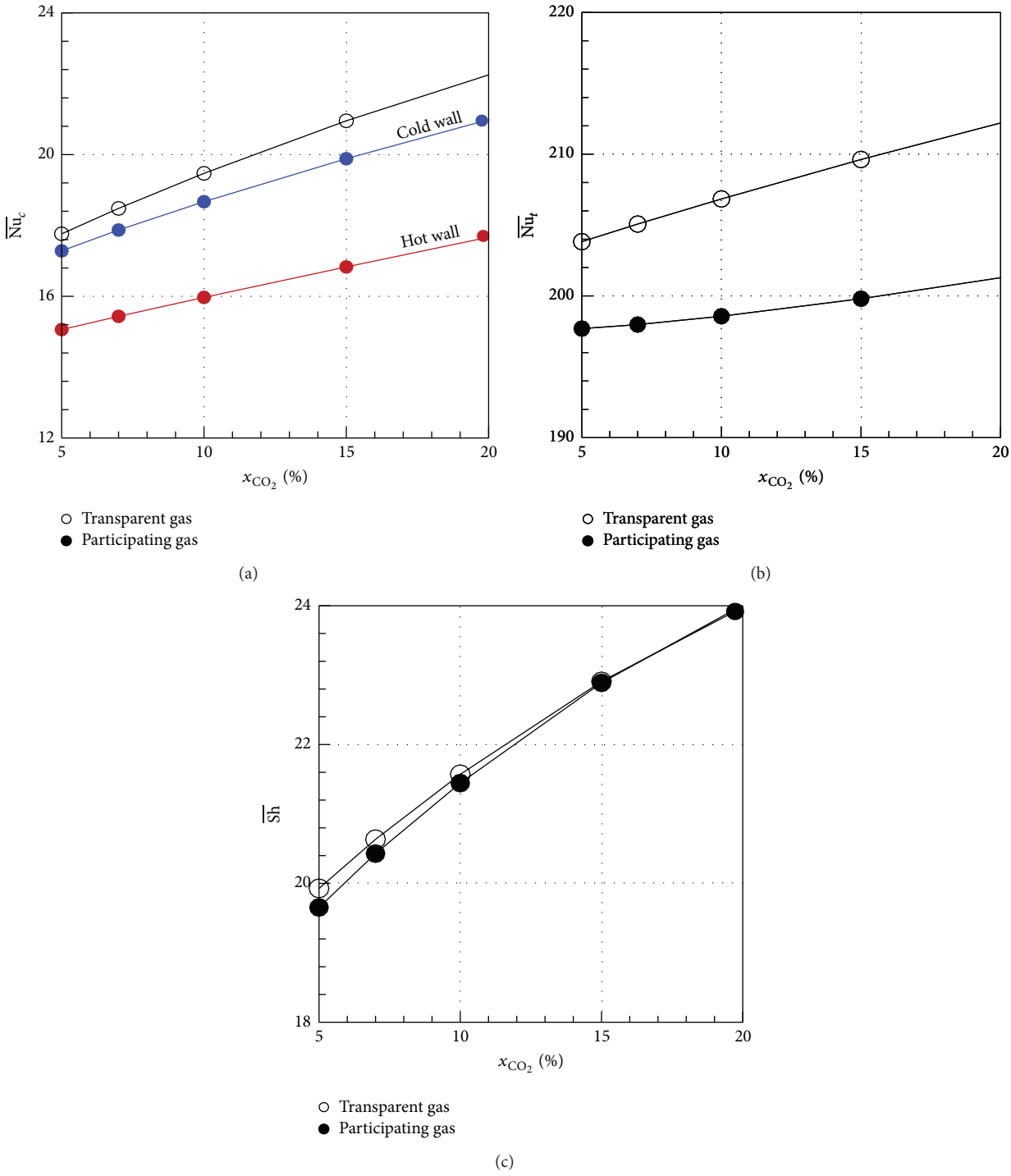

FIGURE 11: Average convective Nusselt number (a), average total Nusselt number (b), and average Sherwood number (c) as a function of molar fraction of CO_2 in cooperating flow.

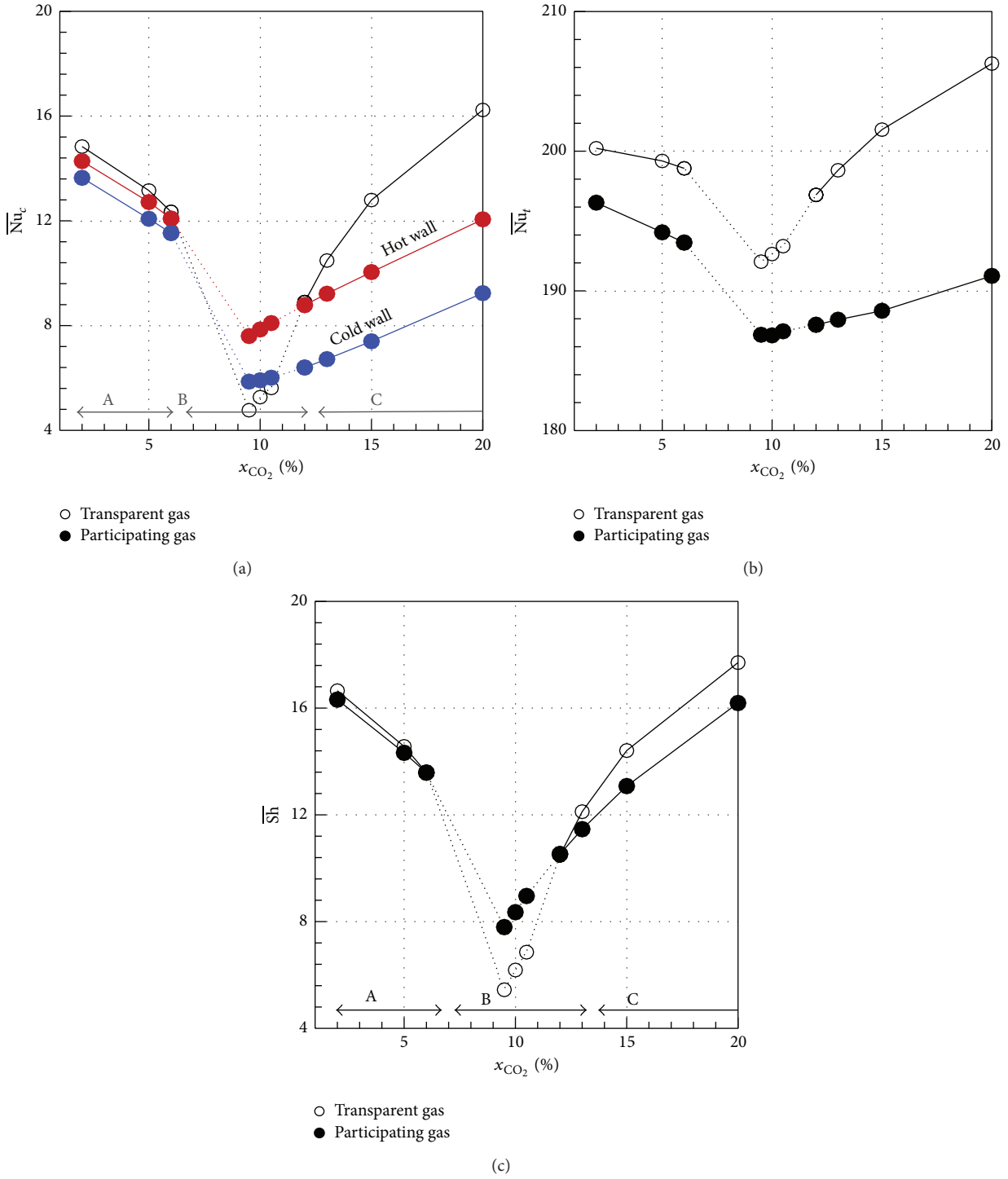

FIGURE 12: Average convective Nusselt number (a), average total Nusselt number (b), and average Sherwood number (c) as a function of molar fraction of CO_2 in opposing flow; A: thermal; B: intermediate regime; C: mass regime.

References

[1] M. Behnia, J. A. Reizes, and G. De Vahl Davis, "Combined radiation and natural convection in a rectangular cavity with a transparent wall and containing a non-participating fluid," *International Journal for Numerical Methods in Fluids*, vol. 10, no. 3, pp. 305–325, 1990.

[2] M. C. Balaji and S. P. Venkateshan, "Interaction of surface radiation with free convection in a square cavity," *International Journal of Heat and Fluid Flow*, vol. 14, no. 3, pp. 260–267, 1993.

[3] N. Ramesh and S. P. Venkateshan, "Effect of surface radiation on natural convection in a square enclosure," *Journal of Thermophysics and Heat Transfer*, vol. 13, no. 3, pp. 299–301, 1999.

[4] H. Wang, S. Xin, and P. L. Quéré, "Étude numérique du couplage de la convection naturelle avec le rayonnement de surfaces en cavité carrée remplie d'air," *Comptes Rendus Mécanique*, vol. 334, no. 1, pp. 48–57, 2006.

[5] G. Lauriat, "Combined radiation-convection in gray fluids enclosed in vertical cavities," *Journal of Heat Transfer*, vol. 104, no. 4, pp. 609–615, 1982.

[6] Z. Wang, M. Yang, L. Li, and Y. Zhang, "Combined heat transfer by natural convection—conduction and surface radiation in an open cavity under constant heat flux heating," *Numerical Heat Transfer Part A*, vol. 60, no. 4, pp. 289–304, 2011.

[7] R. E. Ayachi, A. Raji, M. Hasnaoui, M. Nami, and A. Abdelbaki, "Combined effects of radiation and natural convection in a square cavity submitted to two combined modes of cross gradients of temperature," *Numerical Heat Transfer, Part A: Applications*, vol. 62, no. 11, pp. 905–931, 2012.

[8] A. Yucel, S. Acharya, and M. L. Williams, "Natural convection and radiation in a square enclosure," *Numerical Heat Transfer; Part A: Applications*, vol. 15, no. 2, pp. 261–277, 1989.

[9] Z. Tan and J. R. Howell, "Combined radiation and natural convection in a two-dimensional participating square medium," *International Journal of Heat and Mass Transfer*, vol. 34, no. 3, pp. 785–793, 1991.

[10] G. Colomer, M. Costa, R. Cònsul, and A. Oliva, "Three-dimensional numerical simulation of convection and radiation in a differentially heated cavity using the discrete ordinates method," *International Journal of Heat and Mass Transfer*, vol. 47, no. 2, pp. 257–269, 2004.

[11] W. Zhang, J. Chen, and F. Lan, "A numerical simulation of combined radiation and natural convection heat transfer in a square enclosure heated by a centric circular cylinder," *Heat and Mass Transfer*, vol. 49, no. 2, pp. 233–246, 2013.

[12] J. C. Bratis and J. L. Novotny, "Radiation-convection interaction in the boundary layer regime of an enclosure," *International Journal of Heat and Mass Transfer*, vol. 17, no. 1, pp. 23–36, 1974.

[13] T. Fusegi and B. Farouk, "Radiation-convection interaction of a non-gray gas in a square enclosure," in *Heat Transfer in Fire*, vol. 73, pp. 63–68, ASME-HTD, 1987.

[14] T. Fusegi, K. Ishii, B. Farouk, and K. Kuwahara, "Natural convection-radiation interactions in a cube filled with a nongray gas," *Numerical Heat Transfer; Part A: Applications*, vol. 19, no. 2, pp. 207–217, 1991.

[15] G. Colomer, R. Cònsul, and A. Oliva, "Coupled radiation and natural convection: different approaches of the SLW model for a non-gray gas mixture," *Journal of Quantitative Spectroscopy and Radiative Transfer*, vol. 107, no. 1, pp. 30–46, 2007.

[16] L. Soucasse, P. Rivière, S. Xin, P. L. Quéré, and A. Soufiani, "Numerical study of coupled molecular gas radiation and natural convection in a differentially heated cubical cavity," *Computational Thermal Sciences*, vol. 4, no. 4, pp. 335–350, 2012.

[17] A. Ibrahim, D. Saury, and D. Lemonnier, "Coupling of turbulent natural convection with radiation in an air-filled differentially-heated cavity at Ra = 1.5×109," *Computers and Fluids*, vol. 88, pp. 115–125, 2013.

[18] P. Ganesan and P. Loganathan, "Radiation and mass transfer effects on flow of an incompressible viscous fluid past a moving vertical cylinder," *International Journal of Heat and Mass Transfer*, vol. 45, no. 21, pp. 4281–4288, 2002.

[19] M. N. Borjini, H. B. Aissia, K. Halouani, and B. Zeghmati, "Effect of optical properties on oscillatory hydromagnetic double-diffusive convection within semitransparent fluid," *International Journal of Heat and Mass Transfer*, vol. 49, no. 21-22, pp. 3984–3996, 2006.

[20] V. R. Prasad, N. B. Reddy, and R. Muthucumaraswamy, "Radiation and mass transfer effects on two-dimensional flow past an impulsively started infinite vertical plate," *International Journal of Thermal Sciences*, vol. 46, no. 12, pp. 1251–1258, 2007.

[21] A. Abidi, L. Kolsi, M. N. Borjini, and H. B. Aissia, "Effect of radiative heat transfer on three-dimensional double diffusive natural convection," *Numerical Heat Transfer; Part A: Applications*, vol. 60, no. 9, pp. 785–809, 2011.

[22] M. Rafieivand, *Etude numérique de la convection de double diffusion en présence de rayonnement en cavité rectangulaire [Doctoral thesis]*, University of Poitiers French, Poitiers, France, 1999.

[23] A. Mezrhab, D. Lemonnier, S. Meftah, and A. Benbrik, "Numerical study of double-diffusion convection coupled to radiation in a square cavity filled with a participating grey gas," *Journal of Physics D: Applied Physics*, vol. 41, no. 19, Article ID 195501, 2008.

[24] F. Moufekkir, M. A. Moussaoui, A. Mezrhab, M. Bouzidi, and D. Lemonnier, "Combined double-diffusive convection and radiation in a square enclosure filled with semitransparent fluid," *Computers and Fluids*, vol. 69, pp. 172–178, 2012.

[25] S. Meftah, A. Ibrahim, D. Lemonnier, and A. Benbrik, "Coupled radiation and double diffusive convection in nongray air-CO_2 and air-H_2O mixtures in cooperating situations," *Numerical Heat Transfer, Part A: Applications*, vol. 56, no. 1, pp. 1–19, 2009.

[26] S. Laouar-Meftah, M. Cherifi, D. Lemonnier, and A. Benbrik, "Gas radiation effects on opposing double-diffusive convection in a non-gray air-H_2O mixture," *International Journal of Thermal Sciences*, vol. 77, pp. 38–46, 2014.

[27] A. Ibrahim and D. Lemonnier, "Numerical study of coupled double-diffusive natural convection and radiation in a square cavity filled with A N_2-CO_2 mixture," *International Communications in Heat and Mass Transfer*, vol. 36, no. 3, pp. 197–202, 2009.

[28] M. K. Denison and B. W. Webb, "The spectral line-based weighted-sum-of-gray-gases model in nonisothermal nonhomogeneous media," *Journal of Heat Transfer*, vol. 117, no. 2, pp. 359–365, 1995.

[29] M. K. Denison and B. W. Webb, "Development and application of an absorptionline blackbody distribution function for CO_2," *International Journal of Heat and Mass Transfer*, vol. 38, no. 10, pp. 1813–1821, 1995.

[30] E. N. Fuller, P. D. Schettler, and J. C. Giddings, "A new method for prediction of binary gas-phase diffusion coefficients," *Industrial and Engineering Chemistry*, vol. 58, no. 5, pp. 18–27, 1966.

[31] C. Béghein, F. Haghighat, and F. Allard, "Numerical study of double-diffusive natural convection in a square cavity," *International Journal of Heat and Mass Transfer*, vol. 35, no. 4, pp. 833–846, 1992.